Assessing airflow unsteadiness in the human respiratory tract under different expiration conditions

Hao Jing[1], Haiwen Ge[2], Hui Tang[3], Ali Farnoud[4], Mohammad Saidul Islam[5], Li Wang[6,#], Chenglei Wang[3], Xinguang Cui[1,*]

[1]School of Aerospace Engineering, Huazhong University of Science and Technology, Wuhan, China

[2]Research Center for Intelligent Supercomputing, Zhejiang Laboratory, Hangzhou, China

[3]Department of Mechanical Engineering, The Hong Kong Polytechnic University, Hong Kong, China

[4]School of Mechanical Engineering, University of Adelaide, Adelaide, Australia

[5]School of Mechanical and Mechatronic Engineering, University of Technology Sydney, Sydney, Australia

[6]School of Environmental Science and Engineering, Tianjin University, Tianjin, China

[#]*this author contributes equally as the first author to this work.*

**Corresponding Author, Email: xinguang_cui@mail.hust.edu.cn, Tel:+8619801262181*

ABSTRACT

To enhance the understanding of airflow characteristics in the human respiratory system, the expiratory airflow in a human respiratory tract model was simulated using large eddy simulation and dynamic mesh under different expiration conditions aligned with clinically measured data. The airflow unsteadiness was quantitatively assessed using power spectral density (PSD) and spectral entropy (SE). The following findings were obtained: (1) The airflow is highly turbulent in the mouth-pharynx region during expiration, with its dynamic characteristics being influenced by both the transient expiration flow pattern at mouth piece and the glottis motion. (2) PSD analysis reveals that the expiratory airflow is very unsteady, exhibiting a broad-band attenuation spectrum in the pharynx-trachea region. When only transient expiration or glottis motion is considered, the PSD spectrum changes slightly. When both are ignored, however, the change is significant, with the peak frequency reduced to 10% of the real expiration condition. (3) SE analysis indicates that the airflow transitions into turbulence in the trachea, and there may be multiple transitions in the region of soft palate. The transient expiration or glottis motion alone increases turbulence intensity by 2%-15%, while ignoring both reduces turbulence intensity by 10%-20%. This study implies that turbulence characteristics can be significantly different under different expiratory conditions, and therefore it is necessary to determine the expiratory flow characteristics using clinically measured expiratory data.

Key words: airflow unsteadiness, power spectral density, spectral entropy, clinically expiratory data, large eddy simulation

1. Introduction

Investigating expiratory airflow comes with an improved understanding of the physiological functions of human breathing processes. Sound generation in the laryngeal region is closely linked to glottis motion and unsteady expiration (Voss et al., 2017; Brouns et al., 2007; Zhao et al., 2020). The sensitivity of laryngeal flow to the structure of the larynx and glottis motion motivated studies on the aerodynamic mechanisms during human expiration. Although these physiological characteristics are inherent to human breathing process, most of the previous research (Cui et al., 2018;

Shang et al., 2019; Tabe et al., 2021) assumed a rigid glottis and steady respiratory pattern, which has led to a partial understanding of the airflow dynamics in human respiratory system. Therefore, it is crucial to explore human expiratory airflow characteristics by considering these physiological properties, i.e., the transient breathing pattern and glottis motion.

Since it is difficult to consider physiological factors such as glottis motion in-vitro experiments, computational fluid dynamics (CFD) has been widely used to explore the airflow structure in human airways (Xi et al., 2018; Tabe et al., 2021; Zhao et al., 2021; Nof et al., 2023). For instance, Chen et al. (2022) employed very-large eddy simulations to investigate the influences of glottal profile and cross-sectional area on the upper airway, and noted that the glottal profile mainly affects laryngeal jet shape while the cross-sectional area impacts more on the velocity of the laryngeal jet and turbulence intensity. Voss et al. (2022) used large eddy simulations (LES) to examine the impact of unilateral vocal fold immobility on inhalation, and their findings revealed immobility of the vocal fold can lead to increased laryngeal jet intensity and flow disturbance. Bhardwaj et al (2022) explored the effects of different glottis expansion ratios on transient airflow and particle deposition, and found that static glottis underestimated the total deposition in the bronchial model. However, these studies only examine the inhalation process and the quantities of interest (such as pressure field and particle deposition) due to transitional and turbulence effects, without conducting quantitative analysis on flow regimes.

Up to now, proper orthogonal decomposition (POD) analysis has been used for postprocessing the large amount of airflow data generated by LES simulations to capture the high variability of turbulence. This method decomposes the flow field into several spatially orthogonal modes and sorts them based on the magnitude of their modal energy (eigenvalues), to determine the dominant modes. The classical POD introduced by Lumley (1967) was extended by Sirovich (1987) by considering the temporal component and is also known as snapshot POD (Arànyi et al., 2013). POD has been used to study the airflow characteristics and particle deposition in the human intra-thoracic airways and upper airway during inhalation (Lin et al., 2007; Agnihotri et al., 2014). Abdelsamie et al. (2017) has demonstrated that the spectral entropy obtained by solving the eigenvalue problem for the temporal autocorrelation function can be used to uniquely quantify the flow state and differentiate the laminar, transitional, or turbulent regimes. Specially, Voss et al. (2019) analyzed the airflow state in two specific human respiratory tract using spectral entropy after POD analysis, but ignored the complex glottis motion and transient breathing patterns.

In summary, although extensive research has been conducted on the airflow characteristics of human respiratory system, most of these studies (Cui et al., 2018; Shang et al., 2019; Tabe et al., 2021) simplified the real physiological characteristics of human respiration, which has led to a lack of clarity regarding the unsteadiness appearing in real expiration conditions (i.e., transient expiration and glottis motion). Therefore, in this study, the airflow field in a human respiratory tract model will be simulated using LES considering different expiration conditions. The power spectral density (PSD) and spectral entropy (SE) analyses (Abdelsamie et al., 2017; Voss et al.

2019) will be used to quantify the airflow unsteadiness. To our best knowledge, this is the first application of the POD-based SE analysis in studying airflow unsteadiness in human airway considering real physiological characteristics. The results will enhance our understanding of the physiological functions and aerodynamic mechanisms in human expiratory processes.

2. Numerical method

2.1 Geometry and mesh

As shown in Fig. 1(a), a human respiratory tract model is constructed based on CT (computer tomography) scans. CT scans were obtained from a non-smoking, healthy 25-year-old male volunteer (Cui et al., 2023; Jing et al., 2023). The dynamic glottis region, illustrated in Fig.1 (b), spans from z=-0.11 m to -0.13 m, within which the vocal fold is located in the z=-0.12 m plane, exhibiting maximum displacement. The simulations were conducted using an unstructured mesh primarily comprising hexahedral elements, generated by ANSYS Fluent Meshing. This type of mesh allows high-quality numerical solutions for complex airflows in respiratory airway (Longest et al., 2007). Four different grid configurations were used for grid-independent validation. The details of the final mesh are shown in Fig. 1(c).

2.2 Numerical model

To reveal the airflow characteristics in the respiratory tract model, 4 cases with different expiration conditions were simulated, referred to as Case 1-4, as listed in Table 1. The Generalized Glottis Motion Function (GGMF) (Zhao et al., 2020) based on clinically measured data (Brouns et al., 2007; Tabe et al., 2021) was used for dynamic modeling of glottis motion in Cases 1 (called real expiration) and 2, with a minimum glottal area of 194 mm^2 (i.e., $A_{g,min}$) and an initial glottal area of 206 mm^2 (i.e., $A_g(0)$), the latter being used in the cases of static glottis (Cases 3 and 4). The GGMF considers the motion of the dynamic glottis region as the movement of surface mesh (Zhao et al., 2020; Jing et al., 2023). In this function, the surface mesh moving depends on both time and space and is achieved using in-house C programs. In addition, the transient expiration waveform at the mouth piece obtained from clinical measurement (Brouns et al., 2007; Tabe et al., 2021) was used in Cases 1 and 3. The average flow rate of the transient expiration waveform is 30.6 L/min used in cases of the steady expiration (Cases 2 and 4). The profiles of normalized glottic area and expiratory flow rate throughout one expiratory cycle are presented in Fig. 2.

Table 1. Cases defined with different glottis motion types and breathing waveforms.

Case number	Glottis motion type	Breathing profile	Breathing cycle period (s)	Averaged expiration flow rate (L/min)
Case 1	Dynamic	Unsteady	1.1	30.6
Case 2	Dynamic	Steady	NA	30.6
Case 3	Static	Unsteady	1.1	30.6
Case 4	Static	Steady	NA	30.6

2.3 Simulation setting-ups

LES was adopted to simulate the transient airflow field in the respiratory tract model. The wall-adapting local eddy-viscosity (WALE) model (Ducros et al., 1998; Xi et al., 2015) was used for modeling the subgrid-scale stresses. The numerical simulations were conducted using OpenFOAM 7. Velocity boundary condition was adopted at the mouth piece, pressure boundary conditions were adopted at the bronchial end. The airway wall boundary is defined as no-slip boundary. More simulation details can be referred to Jing et al (2023). It took about four weeks to complete Case 1 using 160 CPU processors in the HPC (High-Performance Computing) cluster in the lab of respiratory multi-phase flows.

Moreover, POD analysis was used to characterize the flow states in the human respiratory tract model. The method of Sirovich (1987) provides further details on the computation of the POD modes. According to Abdelsamie et al (2017), the turbulence intensity can be further assessed by the spectral entropy as a measure of the mode distribution. More details on the POD analysis and the spectral entropy are attached in Appendix A.

3. Verification

Four sets of grids are used for grid independence verification, with 0.67, 3.72, 6.47, and 13.7 million of total grid nodes, respectively. Profiles of average velocity magnitude (U_{mean}) along the polyline in the mid-plane of the model were compared (Fig. A1(a)). As shown in Fig. A1(b), the velocity profile from Mesh-3 agrees with that from Mesh-4 at almost everywhere along the polyline. The difference in the spatially averaged velocity along the polyline between these two cases is only 0.16%, suggesting that the Mesh-3 is sufficient to capture the airflow characteristics in the human respiratory tract model.

The simulation framework utilized in this study has been well validated in our previous work (Jing et al., 2023), in which the simulation results agreed with PIV measurements (Heenan et al., 2003) very well.

4. Results and discussion

The expiratory airflow characteristics at four selected moments, representing the accelerating expiration stage and glottis contraction stage at T_1=0.93 s, the accelerating expiration stage and maximum glottis contraction stage at T_2=1.07 s, the maximum expiration stage and glottis extension stage at T_3=1.33 s, the decelerating expiration stage and glottis extension stage at T_4=1.99 s, respectively, are presented in the following sections. The corresponding Reynolds numbers are Re=288, 1925, 3182, and 288, respectively. In the following discussion, all the presented velocities are normalized by the mouth velocity magnitude.

4.1 Velocity field and vortex structure

In the trachea, the velocity profiles exhibit a plug flow (Martonen et al., 1995) as boundary layers developed along the tracheal surfaces at t=T_1-T_4 for Case 1-4 (Fig. 3). In the glottal region, the airstream passes smoothly over the glottis without any reversed laryngeal jet, although it does accelerate slightly. As the air flows further, a jet-like flow appears nearby the pharynx-larynx junction (except T_1 and T_4 under transient expiration), a clear recirculation zone appears in the lower lobe of the pharynx (except T_4 under transient expiration). When airflow enters the soft palate, the velocity increased due to the reduced cross-sectional area (red color in Fig. 3) and a jet flow is formed at the constricted location. It impacts the roof of the mouth and a recirculation zone appears in the area of lower jaw. These results indicate that expiratory airflow is significantly different from the inspiratory flow (Xi et al., 2018; Zhao et al., 2021), particularly the characteristics of the jet flow and recirculation zones mainly due to the opposite flow directions.

Further, airflow characteristics vary depending on different expiration conditions (Case 1-4) (Fig. 3). For instance, at the accelerating phase (i.e., $t=T_1$), the flow patterns in the mid-plane exhibit similarities between Case 1 and 3. In contrast to Case 1 and 3, the jet at the soft palate is more pulsating in Case 2 and 4, and the area of recirculation zone at the lower lobe of the pharynx is larger. Particularly, the low-velocity flow area in the trachea is much larger at this moment in Case 4 (Fig. 3(d)). At $t=T_2$, the airflow in the mid-plane for Case 2 is the most unsteady, and the low-velocity flow area in the trachea under steady expiration is significantly larger than that under transient expiration, i.e., Case 1 vs. Case 2, Case 3 vs. Case 4 (Fig. 3). The glottis motion increases the recirculation zone at the lower lobe of the pharynx, as revealed by comparing Case 1 with Case 3, or Case 2 with Case 4. At $t=T_3$, the low-velocity flow area in the trachea for all cases increases compared to that at $t=T_2$. At $t=T_4$, the airflow at the entire upper airway in Case 1 and 3 is extremely unsteady compared to that in Case 2 and 4. Moreover, the recirculation zone at the lower lobe of the pharynx disappears in Case 1 and 3. Especially, due to the flow lingering effect at the same Reynolds number, the flow field at $t=T_4$ in Case 1 and 3 is more unsteady than that at $t=T_1$, which is not obvious in Case 2 and 4 (Fig. 3). These findings indicate that both the expiratory pattern and the glottis motion have impacts on the flow field in the upper airway. Ignoring transient expiration will lead to inaccurate predictions in expiratory airflow behaviors, while ignoring glottis contraction will alter the degree of variation in the recirculation zone over time.

Following the analysis of velocity field above, the vortical characteristics are analyzed using the Ω-criterion method (Liu et al. 2018). As seen in Fig. 4, large-scale vortex structures mainly exist in the mouth-pharynx region. For the transient expiration pattern (Case 1 and 3), the distribution range and intensity of vortex structures are significantly varied at T_2 and T_3. In contrast, under steady inspiration (Case 2 and 4), they are insignificantly varied over time, while they are wider and stronger in Case 4 than in Case 2. This finding affirms that glottis contraction, during steady expiration, increases kinetic energy loss and subsequently intensifies the dissipation of large-scale vortex structures (Xi et al., 2018). However, it becomes weaker in case of transient expiration pattern (Case 1 and 3). These results confirm that variations in vortex structures are primarily influenced by the expiration pattern, while the impact of glottis motion is relatively weak, especially under transient expiration.

Overall, the qualitative analysis demonstrates that the airflow in the mouth-pharynx during expiration is highly turbulent and unstable. The dynamic characteristics of the airflow structures in the mouth-pharynx are caused by the combined effects of geometric structure induced turbulence, transient expiratory pattern, and glottis dynamics. The expiratory flow pattern at the mouth exerts a greater influence on the dynamics of bulk flow and vortex structures in the upper airway compared to the glottis motion. Glottis contraction can increase the dissipation of vortex structures by maximizing kinetic energy loss. Assuming a static glottis or a steady expiratory pattern leads to significant variations of turbulence structures in the mainstream and recirculation regions. In the scenario where both a static glottis and a steady expiratory flow rate are assumed, the turbulence structures will significantly differ from those observed in the real situation.

4.2 PSD analysis

The Power Spectral Density (PSD) is adopted to show the frequency of unsteady airflow throughout the present airway model. The details about the PSD method can be found in Appendix B. As seen in Fig. 5, the PSD spectra at three monitoring points A-C located at pharynx, glottis and trachea follow a similar trend in all cases, which span in a broad frequency range. The PSD can be approximated with a -5/3 slope in the so-called inertial subrange for high Reynolds numbers (Bernate et al., 2017). The slope then gradually changes to -10/3 and finally becomes -7, indicating the dominance of viscous forces. Comparing the PSD characteristics at the three locations in each case (Fig. 5), it can be seen that during the expiration process, the PSD profiles at the trachea is closer to those at the glottis, while the magnitude range and maximum frequency of PSD at the pharynx are significantly larger. This phenomenon is consistent with the flow fields shown in Section 4.1 (Fig. 3). All PSDs reveal one important fact that the expiratory airflow is very unsteady, exhibiting broad-band attenuation spectrum in the pharynx-trachea region, while it is even more unsteady at the pharynx.

By comparing the PSD spectra across different cases, it can further reveal the influence of expiration conditions on the turbulent characteristics in the respiratory tract. As shown in Fig. 5(a)-(d), the significant differences of PSD among the four cases are the maximum PSD frequency and values at low frequencies (Fig. 5). For instance, the low-frequency PSD values at the monitoring points are reduced when only transient exhalation is ignored (Case 2). The low-frequency PSD values at these points in Case 1 is about 10^{-1}, while in Case 2 they are between 10^{-2} and 10^{-4}. The maximum frequency is also reduced: the value in Case 2 is about 80% of the value in Case 1 (Fig. 5). When only the glottis motion (Case 3) is ignored, the variations of PSD profiles are small, with the main difference between point B and C located at a frequency of 25 1/s (Fig. 5 (c)). At this frequency, the relative difference of PSD values at these two points in Case 3 is significant, approximately 225% of that in Case 1. When neither the glottis motion or the transient expiration is considered (Case 4), the maximum frequency of PSD is about 10% of Case 1, and the low-frequency PSD value is also low, about 10^{-3}, which is the most different with Case 1 among all cases. Overall, the above results indicate that there is a significant deviation in the PSD characteristics in the upper airway when the transient expiration and the glottis motion are ignored compared to the real expiration. The impact of expiratory pattern and glottis motion on the PSD varies at different positions, but overall, the expiratory flow pattern at the mouth piece has a greater influence.

4.3 SE analysis

Although the PSD method can well-detect strong turbulence in different kinds of flows (Varghese et al. 2007; Janiga 2014), it cannot clearly distinguish transitional flow. Therefore, the spectral entropy (SE) was used to quantitatively demonstrate the turbulent characteristics as the way used in Abdelsamie et al. (2017) and Voss et al. (2017). Fig. 6 exhibits the SE along the flow direction for every sampling plane in the human respiratory tract model (from the left upper lobe to the oral cavity) for the four cases, with the sampling positions shown in Fig.1 (d). It can be seen that the evolution progress of airflow is similar for all cases. For instance, the SE value is less than 0.5 in the bronchial airway from 0 m to 0.05 m (calculated from the point D in Fig. 1(d), hereafter) for all cases, indicating a laminar airflow. Afterwards, it transits from laminar to turbulent in the trachea region, confirmed by the SE value ranging from 0.7 to 1.1 near the end of the trachea (from 0.05 m to 0.06 m). It is worth noting that SE in Voss et al. (2017) is approximately 0 in the trachea, which is possibly because their airway model doesn't include the bronchial tree, which leads to smoother flow in the trachea. The SE sharply increases until 0.07 m, signifying that turbulence primarily develops nearby in the junction of larynx and trachea (Fig. 6). Afterwards, the SE begins to decrease and then fluctuates between 0.15 m to 0.22 m, possibly due to the curvature of the trachea (Case 1-4). A valley of SE appears at 0.225 m due to the glottis motion, with Case 1-4 as low as 1.9, 2.0, 1.8, 1.5, respectively. From 0.225 m to 0.317 m, the SE consistently maintains at a high level with an average value of ~2.2 for Case 1-4, albeit with some fluctuations (Fig. 6). This indicates that turbulence is well-maintained in the pharynx region. SE decreases to ~1.1 at 0.328 m, then increases to ~2.0 at 0.352 m, and finally maintains a high level until 0.4 m (Case 1-4). These findings suggest that during expiration, the airflow in the bronchi is laminar, with transitions occurring at the end of the trachea, and turbulence developing in the trachea. The flow in the pharynx-larynx and mouth is very unsteady, and there may be multiple transitions in the soft palate.

Furthermore, distributions of SE are different across all cases, as seen in Fig. 6.

For instance, SE in the trachea slightly increases when transient expiration or glottis motion is ignored (Case 2 and 3), while it significantly decreases ignoring both of them (Case 4), which can be demonstrated by that the averaged spectral entropy between 0.08 m-0.22 m is 2.24, 2.29, 2.26, and 2.09 for Case 1-4, respectively (Fig. 6). Similar phenomena are also observed in the glottis where SE are 1.85, 1.91, 2.13, and 1.52 for Case 1-4, respectively. In the pharynx-larynx region, the glottis motion reduces flow unsteadiness under transient expiration, leading to lower SE in Case 1 compared to Case 3 (Fig. 6). Simultaneously, the SE is higher in this region for Case 2 compared to Case 4 (Fig. 6). This indicates that the glottis motion results in increased turbulence in this region under steady expiration. Interestingly, SE are 1.10, 1.20, 1.16, and 0.91 at the position of 0.328 m located in soft palate for Case 1-4, respectively. This implies that turbulence intensity in the upper airway increases when either the glottis motion or the transient expiration is ignored, while when both are ignored, the turbulence intensity will be weaker.

In summary, during expiration, the airflow in the bronchi is laminar, with transitions occurring at the end of the trachea, and turbulence developing in the trachea. The flow in the pharynx-larynx and mouth is very unsteady, and there may be multiple transitions in the soft palate. When ignoring glottis motion or transient expiration, the turbulence intensity in most positions of the upper airway will increase, about 102%-115% of the values at real expiration condition, while when both are ignored, the turbulence intensity will be weak, about 80%-90% of that at real expiration condition.

5. Conclusions

In this work, we adopted PSD and SE to investigate the airflow unsteadiness in a human respiratory tract model under different expiration conditions. The airflow structures are highly turbulent and unstable in the mouth-pharynx region during expiration, which is caused by the combined effects of geometry-induced turbulence, the transient expiratory flow rate, and glottis motion. Analysis of PSD demonstrates that the expiratory airflow is very unsteady, exhibiting broad-band attenuation spectra in the pharynx-trachea region. Ignoring either transient expiration or glottis motion alone will result in varying PSD profiles, and when both are ignored, the maximum frequency will be significantly reduced, about 10% of the real expiration condition. Spectral entropy analysis indicates that laminar flow occurs in the bronchi and develops into turbulence in the trachea, and there may be multiple transitions in the soft palate. Ignoring glottis motion or transient expiration will increase turbulence intensity by 2%-15%, while ignoring both will reduce turbulence intensity by 10%-20%. Therefore, it is necessary to adopt precise expiratory data when studying the properties of airflow structures in the human respiratory system, and more physiological data should be considered to obtain more realistic respiratory airflow characteristics.

Conflict of interest statement

The authors declare no conflict of interest.

Acknowledgments

The authors acknowledge the support of National Natural Science Foundation of China (Grant No.12172146).

Appendix

A. POD analysis and spectral entropy

The $\boldsymbol{U}$ matrix is constituted by the velocity fluctuation components (u', v', w') for each mesh element point (x_i, y_i, z_i) for the N instantaneous flow fields. Hence, $\boldsymbol{U}$ is defined as follows:

$$\boldsymbol{U} = \left[u'^{(1)} u'^{(2)} \cdots u'^{(N)} \right], \tag{A1}$$

where the velocity fluctuation component is extracted from the decomposition of the velocity field

$$u'(x,y,z,t) = u(x,y,z,t) - \bar{u}(x,y,z,t), \tag{A2}$$

The POD is performed to determine the eigenvalues $\lambda^{(k)}$ and eigenvectors $\boldsymbol{A}^{(k)}$ of the cross-correlation matrix $\boldsymbol{C}$=(1/N)$\boldsymbol{U}^{\mathrm{T}}\boldsymbol{U}$ by $\boldsymbol{C}\boldsymbol{A}^{(k)} = \lambda^{(k)}\boldsymbol{A}^{(k)}$. The POD modes ($\boldsymbol{\varphi}^{(k)}$) are then computed from the eigenvectors and dataset as follows:

$$\boldsymbol{\varphi}^{(k)} = \frac{\sum_{n=1}^{N} \boldsymbol{A}^{(k)(n)} \boldsymbol{u}^{(n)}}{\left\| \sum_{n=1}^{N} \boldsymbol{A}^{(k)(n)} \boldsymbol{u}^{(n)} \right\|}, \tag{A3}$$

where $\|-\|$ denotes the Frobenius norm.

The relative energy $P^{(k)}$ is computed based on the corresponding eigenvalue, after ordering them in decreasing order based on $\lambda^{(k)}$, as:

$$P^{(k)} = \frac{\lambda^{(k)}}{\sum_{k=1}^{M} \lambda^{(k)}}, \tag{A4}$$

where $M \le N$ is the number of modes retained in the analysis. Then, the spectral entropy can be determined as:

$$SE = -\sum_{k=1}^{M} P^{(k)} \ln P^{(k)} . \qquad \text{(A5)}$$

B. Power spectral density

PSD is a frequency domain analysis, which shows the strength of the variation in energy as a function of frequency. To calculate the PSD, the signal is first sampled to obtain a discrete time sequence x(n). Then, the FFT is applied to the sequence.

$$X(k) = \sum_{n=0}^{N-1} x(n) \exp(-j \frac{2\pi}{N} kn) \quad k=0,\ 1,\ 2,\ \ldots,\ N-1. \qquad \text{(A6)}$$

where $X(k)$ is the Fourier transform coefficient calculated from the FFT algorithm. Power spectral density is calculated from the Fourier transform coefficients at each point.

References

Arànyi, P., Janiga, G., et al., 2013. Analysis of different POD methods for PIV measurements in complex unsteady flows. International Journal of Heat and Fluid Flow. 43, 204-211. https://doi.org/10.1016/j.ijheatfluidflow.2013.07.001

Agnihotri, V., Ghorbaniasl, G., et al., 2014. On the multiple LES frozen field approach for the prediction of particle deposition in the human upper respiratory tract. Journal of Aerosol Science. 68, 58-72. https://doi.org/10.1016/j.jaerosci.2013.11.001

Abdelsamie, A., Janiga, G., et al., 2017. Spectral entropy as a flow state indicator. International Journal of Heat and Fluid Flow. 68, 102-113. https://doi.org/10.1016/j.ijheatfluidflow.2017.09.013

Brouns, M., Verbanck, S., et al., 2007. Influence of glottic aperture on the tracheal flow. Journal of Biomechanics. 40(1), 165-172. https://doi.org/10.1016/j.jbiomech.2005.10.033

Bhardwaj, S., Koullapis, P., et al., 2022. Fate of inhaled aerosols under the influence of glottal motion in a realistic in silico human tracheobronchial tree model. European Journal of Pharmaceutical Sciences. 173. https://doi.org/10.1016/j.ejps.2022.106172

Bernate, J.A., Geisler, T.S., Padhy, S., 2017. Study of the flow unsteadiness in the human airway using large eddy simulation. Physical Review Fluids. 2. https://doi.org/10.1103/PhysRevFluids.2.083101

Cui, X.G., Wu. W., et al., 2018. Numerical study of the airflow structures in an idealized mouth throat under light and heavy breathing intensities using large eddy simulation. Respiratory Physiology & Neurobiology. 248, 1-9. https://doi.org/10.1016/j.resp.2017.11.001

Chen, W.J., Wang, L., et al., 2022. Numerical study of the impact of glottis properties on the airflow field in the human trachea using V-LES. Respiratory Physiology & Neurobiology. 295. https://doi.org/10.1016/j.resp.2021.103784

Cui, X.G., Song, W., et al., 2023. Numerical investigations of the micro lunar dust particles deposition in the human oral respiratory airway. Journal of Hazardous Materials. 448. https://doi.org/10.1016/j.jhazmat.2023.130886

Ducros, F., Nicoud, F., et al., 1998. Wall-Adapting Local Eddy Viscosity Models for Simulations in Complex Geometries. Oxford University Computing Laboratory, Oxford, UK. 293-299

Heenan, A.F., Matida, E., et al., 2003. Experimental measurements and computational modeling of the flow field in an idealized human oropharynx. Experiments in Fluids. 35(1), 70-84. https://doi.org/10.1007/s00348-003-0636-7

Jing, H., Ge, H.W., et al., 2023. Large eddy simulation study of the airflow characteristics in a human whole-lung airway model. Physics of Fluids. 35. https://doi.org/10.10163/5.0156310

Janiga, G., 2014. Large Eddy simulation of the FDA benchmark nozzle for a Reynolds number of 6500. Computers in Biology & Medicine. 47, 113-119. https://doi.org/10.1016/j.combiomed.2014.01.004

Lumley, J.L., 1967. The structure of inhomogeneous turbulent flows. In: Yaglom, A.M., Tatarski, V.I. (eds.) Atmospheric Turbulence and Radio Propagation. 166-178.

Lin, C.L., Tawhai, M.H., et al., 2007. Characteristics of the turbulent laryngeal jet and its effect on airflow in the human intra-thoracic airways. Respiratory Physiology & Neurobiology. 157(2-3), 295-309. https://doi.org/10.1016/j.resp.2007.02.006

Longest, P.W., Vinchurkar, S., 2007. Effects of mesh style and grid convergence 770 on particle deposition in bifurcating airway models with comparisons to experimental data. Medical Engineering and Physics. 29(3), 350-366. https://doi.org/10.1016/j.medengphy.2006.05.012

Liu, C.Q., Gao, Y.S., et al., 2018. Rortex-A new vortex vector definition and vorticity tensor and vector decompositions. Physics of Fluids. 30(3). https://doi.org/10.10163/1.5023001

Martonen, T.B., Zhang, Z., and Yang, Y., 1995. Particle diffusion with entrance effects in a smooth-walled cylinder. Journal of Aerosol Science. 27, 139-150. https://doi.org/10.1016/0021-8502(95)00530-7

Nof, E., Bhardwaj, S., et al., 2023. In vitro-in silico correlation of three-dimensional turbulent flows in an idealized mouth-throat model. Plos Computational Biology. 19(3). https://doi.org/10.1371/journal.pcbi.1010537

Shang, Y., Dong, J., et al., 2019. Detailed computational analysis of flow dynamics in an extended respiratory airway model. Clinical Biomechanics. 61, 105-111. https://doi.org/10.1016/j.clinbiomech.2018.12.006

Sirovich, L., 1987. Turbulence and the dynamics of coherent structures. Part 1: Coherent structures. Quat Appl Math. 45(3), 561-571.

Tabe, R., Rafee, R., et al., 2021. Investigation of airflow at different activity conditions in a realistic model of human upper respiratory tract. Computer Methods in Biomechanics and Biomedical Engineering. 24(2), 173-187. https://doi.org/10.1080/10255842.2020.1819256

Voss, S., Arens, C., Janiga, G., 2019. Assessing transitional air flow during human expiration from large eddy simulations based on spectral entropy. Flow Turbulence Combust 102, 117-128. https://doi.org/10.1007/s10494-018-9894-6

Voss, S., Vutlapalli, S.C., et al., 2022. CFD simulations of inhalation through a subject specific human larynx-Impact of the unilateral vocal fold immobility. Computers in Biology and Medicine. 143. https://doi.org/10.1016/j.compbiomed.2022.105243

Varghese, S.S, Frankel, S.H., Fischer, P.H., 2007. Direct numerical simulation of stenotic flows. Part 1: Steady flow. Journal of Fluid Mechanics. 582, 253-280. https://doi.org/10.1017/S0022112007005848

Xi, J.X., April Si, X.H., et al., 2018. Effects of glottis motion on airflow and energy expenditure in a human upper airway model. European Journal of Mechanics/B Fluids. 72, 23-37. https://doi.org/10.1016/j.euromechflu.2018.04.011

Xi, J., Kim, J., et al., 2015. CFD Modeling and Image Analysis of Exhaled Aerosols Due to a Growing Bronchial Tumor: Towards Non-Invasive Diagnosis and Treatment of Respiratory Obstructive Diseases. Theranostics. 5(5), 443-455. https://doi.org/10.7150/thno.11107

Zhao, J.N., Feng, Y., et al., 2020. Glottis motion effects on the particle transport and deposition in a subject-specific mouth-to-trachea model: A CFPD study. Computers in Biology and Medicine.

116. https://doi.org/10.1016/j.compbiomed.2019.103532

Zhao, J.N., Feng, Y., et al., 2021. Prediction of airway deformation effect on pulmonary air particle dynamics: A numerical study. Physics of Fluids. 33. https://doi.org/10.1063/5.0065309

Figure Captions

Fig. 1: The geometrical structures of a human respiratory tract model and its local mesh details. (a) Geometrical structures of the human respiratory tract model, RMB displays the right main bronchus, LMB displays the left main bronchus, the blue region displays the glottis region. (b) The z-direction span of the glottis region and the changes in the cross-sectional area of the glottis at three different times. (c) Schematic plots of the grids at the glottis region. (d) Sample points along the flow direction from the bronchus to the mouth.

Fig. 2: Normalized dynamic glottis area and the airflow rate at mouth piece from clinically measured data (Brouns et al., 2007; Tabe et al., 2021) and prediction with the GGMF functions (Zhao et al., 2020), where A_g* is the normalized area, Q_{out}* is the normalized expiration flow rate, and the expiratory period is 1.1 s.

Fig. 3: The normalized instantaneous velocity magnitude at the mid-plane at t=T_1-T_4 for Case 1-4 during the expiratory process. The u and U_m present the instantaneous velocity magnitude inside the airway model and the velocity magnitude at the mouth piece, respectively. Case 1 represents the transient expiratory pattern and glottis motion (a), Case 2 represents the steady expiratory pattern and glottis motion (b), Case 3 represents the transient expiratory pattern and rigid glottis (c) and Case 4 represents the steady expiratory pattern and rigid glottis (d).

Fig. 4: The vortex structures with Ω=0.52 for Case 1-4 at all four times T_1-T_4. Case 1 (a)-Case 4 (d) refer to the description in the caption of Fig. 3.

Fig. 5: Power spectral density (PSD) calculated from the velocity fluctuation at point A-C for Case 1-4, where point A-C displays the locations of the pharynx, larynx and trachea, respectively. Case 1 (a)-Case 4 (d) refer to the description in the caption of Fig. 3.

Fig. 6: The variation of spectral entropy (SE) with the distance from the left upper lobe to the mouth for Case 1-4. Case 1-4 refer to the description in the caption of Fig. 3.

Figure Captions: Appendix

Fig. A1: (a) The polyline (red color) in the upper airway for digging the airflow velocity, where the gray plane is the location of mid-plane, and a-h are endpoints on the polyline. (b) Umean profiles along the polyline from the four sets of grids, where 0 m is location near the center at the mouth outlet.

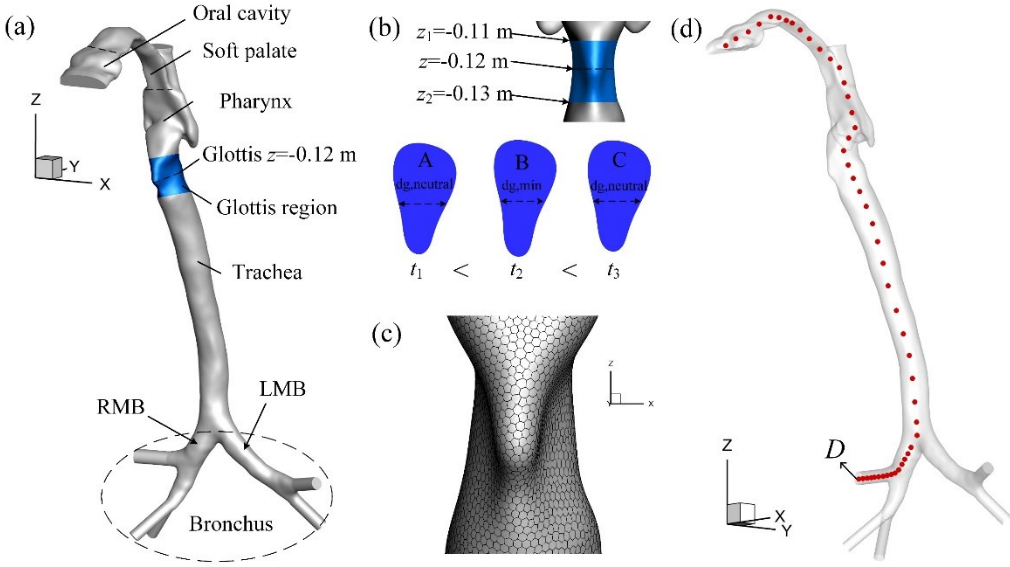

(a)
Oral cavity
Soft palate
Pharynx
Glottis z=-0.12 m
Glottis region
Trachea
RMB
LMB
Bronchus
Z
Y
X
(b)
z_1=-0.11 m
z=-0.12 m
z_2=-0.13 m
A
B
C
dg,neutral
dg,min
dg,neutral
t_1 < t_2 < t_3
(c)
(d)
D

Fig. 1

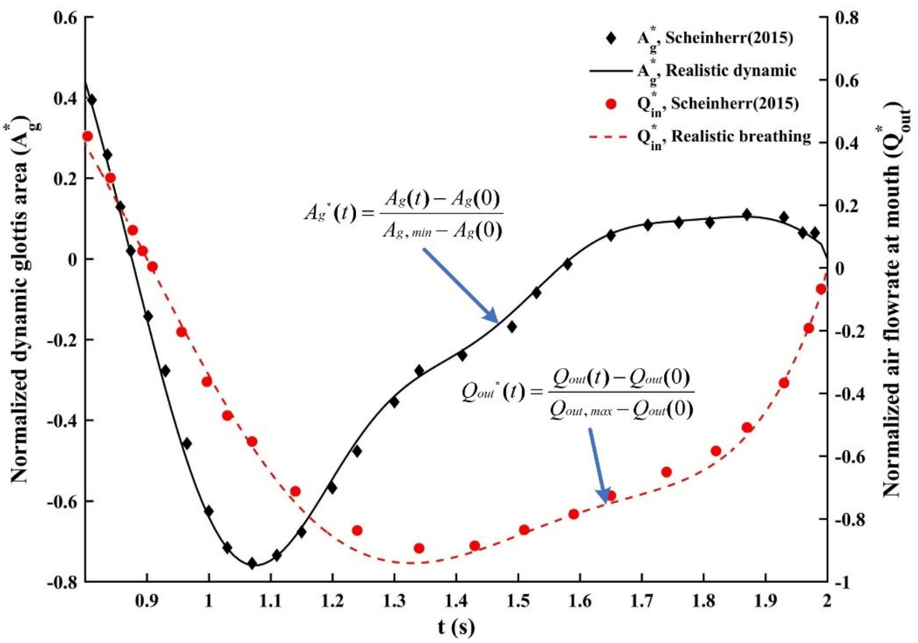

Normalized dynamic glottis area (A_g^*)
Normalized air flowrate at mouth (Q_{out}^*)
t (s)
A_g^*, Scheinherr(2015)
A_g^*, Realistic dynamic
Q_{in}^*, Scheinherr(2015)
Q_{in}^*, Realistic breathing
$A_g^*(t) = \frac{A_g(t) - A_g(0)}{A_{g,min} - A_g(0)}$
$Q_{out}^*(t) = \frac{Q_{out}(t) - Q_{out}(0)}{Q_{out,max} - Q_{out}(0)}$

Fig. 2

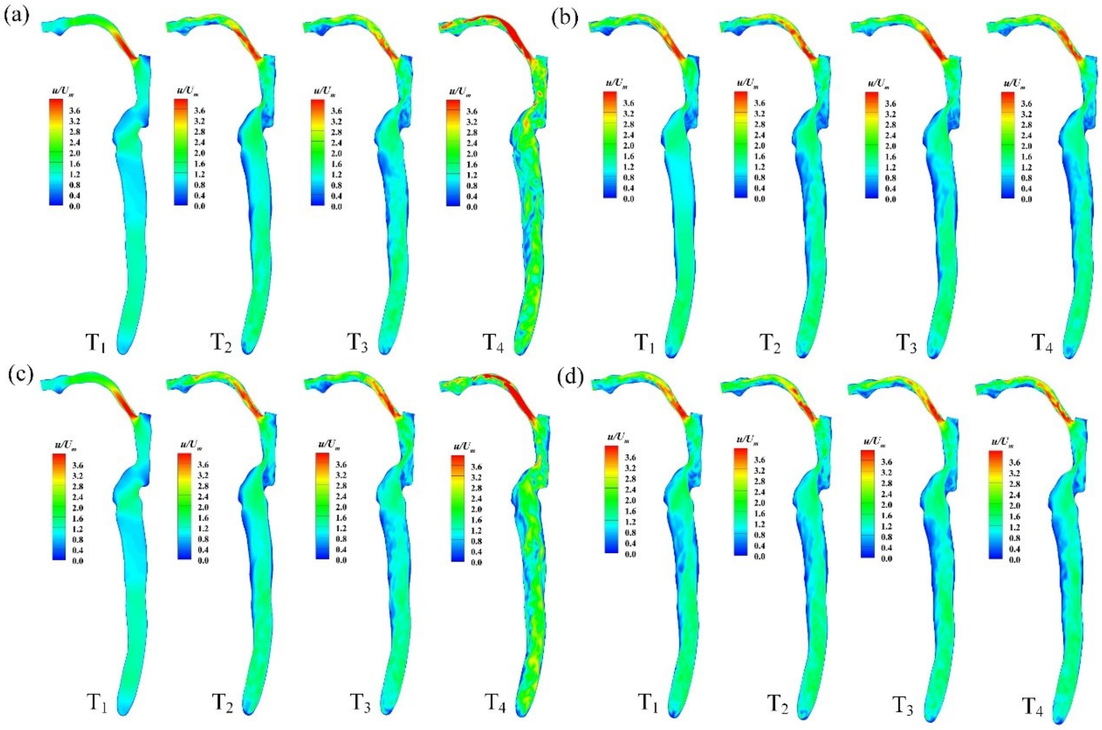

Fig. 3

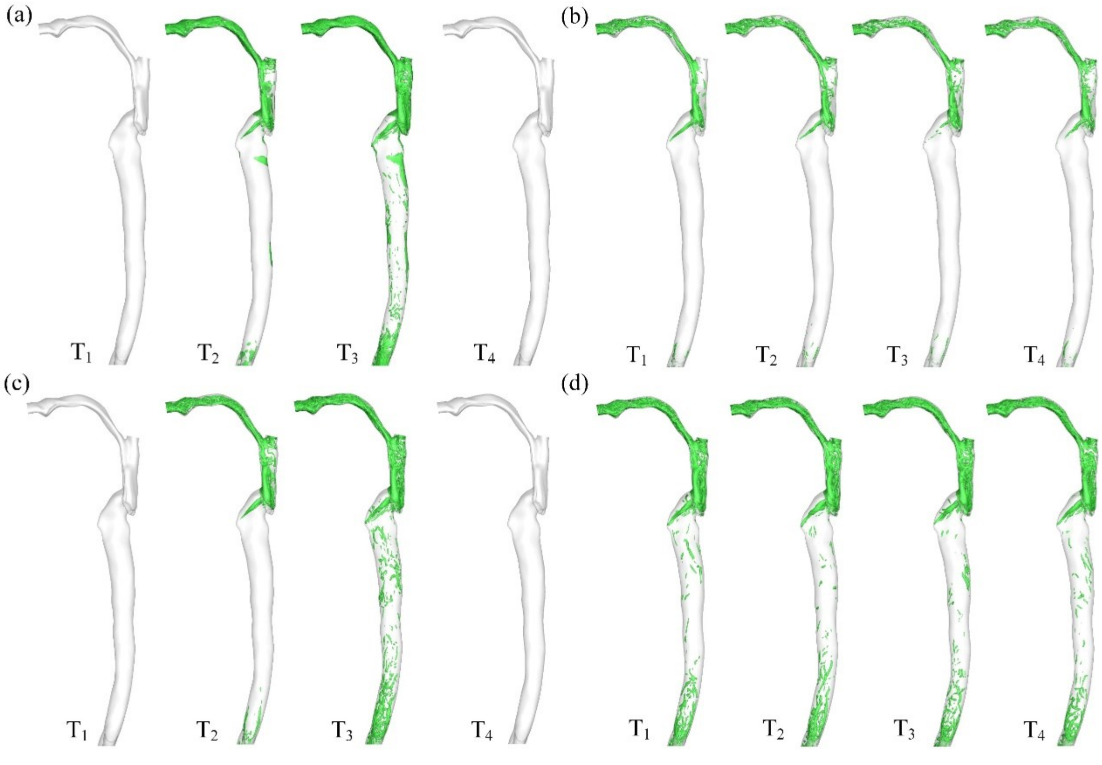

Fig. 4

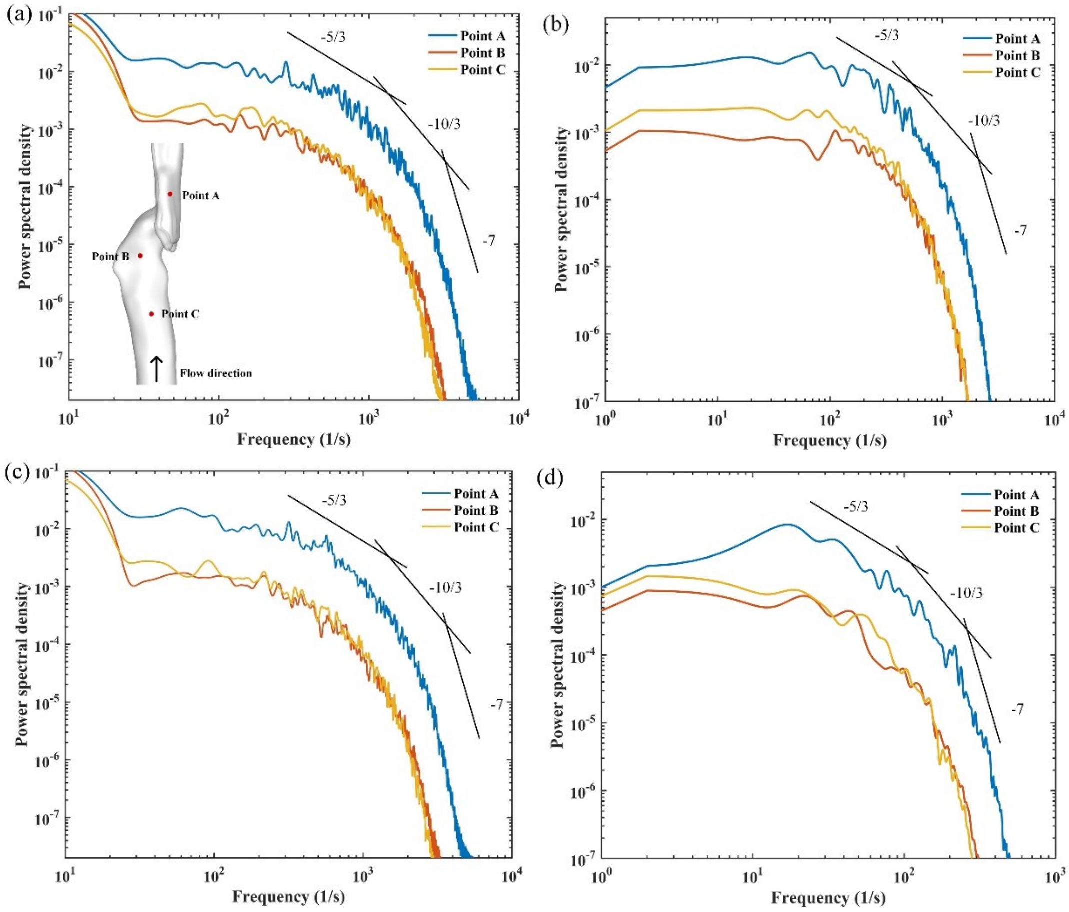

(a)
(b)
(c)
(d)
Point A
Point B
Point C
-5/3
-10/3
-7
Power spectral density
Frequency (1/s)
Flow direction

Fig. 5

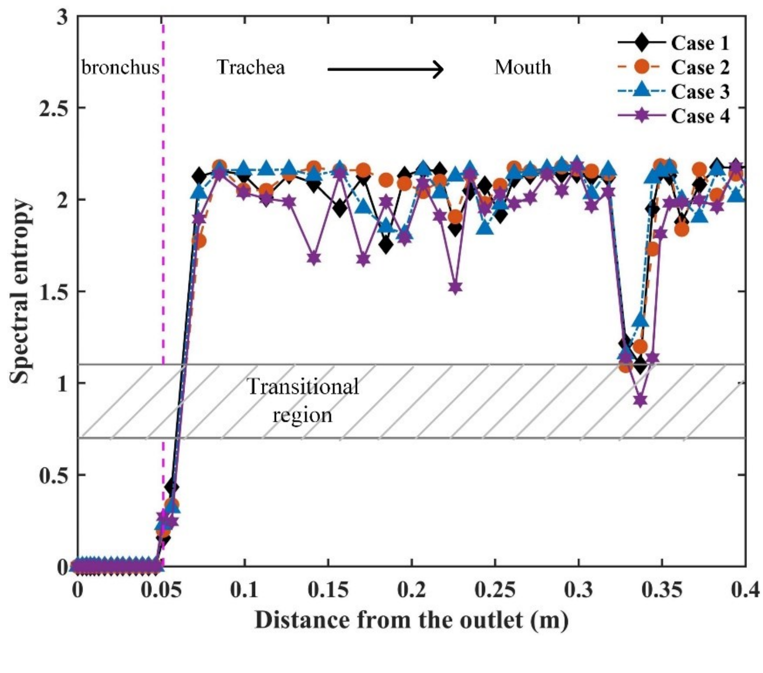

bronchus
Trachea
Mouth
Case 1
Case 2
Case 3
Case 4
Transitional region
Spectral entropy
Distance from the outlet (m)

Fig. 6

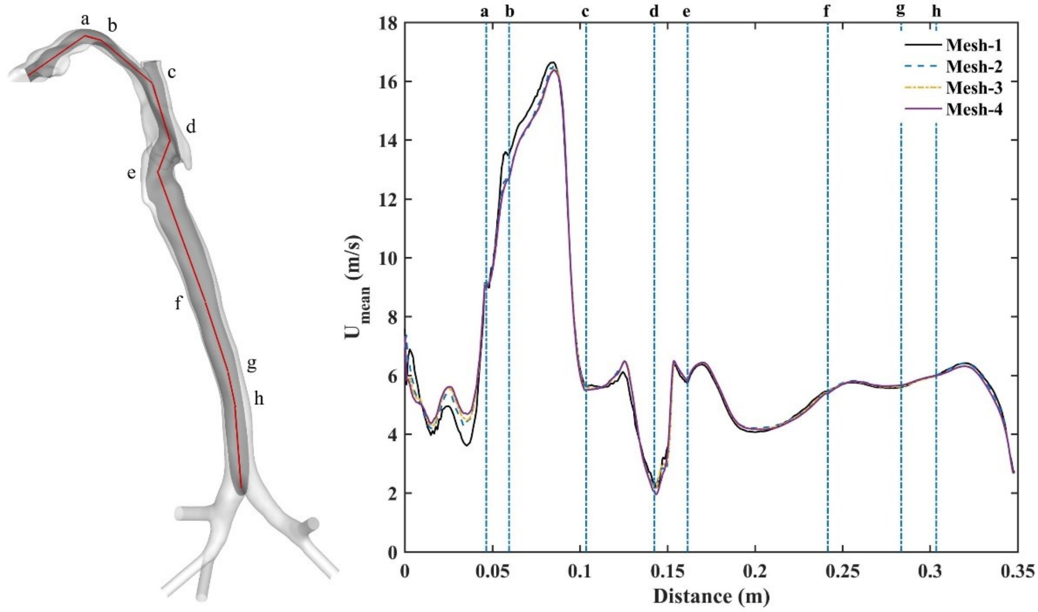
a
b
c
d
e
f
g
h
Mesh-1
Mesh-2
Mesh-3
Mesh-4
U_{mean} (m/s)
Distance (m)
0
0.05
0.1
0.15
0.2
0.25
0.3
0.35
0
2
4
6
8
10
12
14
16
18

(a) (b)

Fig. A1